Talanta 105 (2013) 244–249

Contents lists available at SciVerse ScienceDirect

Talanta

journal homepage: www.elsevier.com/locate/talanta

Determination of total viable count (TVC) in chicken breast fillets by near-infrared hyperspectral imaging and spectroscopic transforms

Yao-Ze Feng, Da-Wen Sun *

FRCFT Group, School of Biosystems Engineering, University College Dublin, National University of Ireland, Agriculture and Food Science Centre, Belfield, Dublin 4, Ireland

ARTICLE INFO

Article history:
Received 28 June 2012
Received in revised form
14 November 2012
Accepted 19 November 2012
Available online 27 November 2012

Keywords:
Chemical imaging
Near-infrared
Chemometrics
Absorbance
K–M
Spoilage
Chicken

ABSTRACT

Near infrared (NIR) hyperspectral imaging (HSI) and different spectroscopic transforms were investigated for their potential in detecting total viable counts in raw chicken fillets. A laboratory-based pushbroom hyperspectral imaging system was utilized to acquire images of raw chicken breast fillets and the resulting reflectance images were corrected and transformed into hypercubes in absorbance and Kubelka–Munck (K–M) units. Full wavelength partial least regression models were established to correlate the three spectral profiles with measured bacterial counts, and the best calibration model was based on absorbance spectra, where the correlation coefficients (R) were 0.97 and 0.93, and the root mean squared errors (RMSEs) were 0.37 and 0.57 log10 colony forming units (CFU) per gram for calibration and cross validation, respectively. To simplify the models, several wavelengths were selected by stepwise regression. More robustness was found in the resulting simplified models and the model based on K–M spectra was found to be excellent with an indicative high ratio of performance to deviation (RPD) value of 3.02. The correlation coefficients and RMSEs for this model were 0.96 and 0.40 log10 CFU per gram as well as 0.94 and 0.50 log10 CFU per gram for calibration and cross validation, respectively. Visualization maps produced by applying the developed models to the images could be an alternative to test the adaptability of a calibration model. Moreover, multi-spectral imaging systems were suggested to be developed for online applications.

1. Introduction

Meats are sources of protein, essential amino acids and a wide variety of micronutrients that are valuable for human nutrition and health [1]. As meats are highly perishable, it is necessary to develop innovative techniques such as refrigeration methods [2–7] and processes [8–12] to enhance their quality and safety, it is equally important to develop novel detection methods to ensure food safety. Compared to red meat, poultry meat is more affordable. The quality and safety of chicken meat rely on its physical, chemical and biological conditions [13], among which the third is of the most concern. Currently, for detection and enumeration of spoilage bacteria, there are over 40 methods available, including microscopy-based enumeration methods [14,15], adenosine triphosphate (ATP) bioluminescence tests [16,17], electrical-phenomenon-based protocols [18] and, among others, immunological or molecular biotechnology, such as polymerase chain reaction (PCR) and enzyme-linked immunosorbent assay (ELISA) [19–23]. However, fast and automatic methods for precise prediction of bacterial loads in chicken meat are rare and urgently needed in the poultry industry for efficient management.

Recent decades have seen booming applications of vibrational spectroscopy in fields like agriculture [24], food [25–27], environment [28,29], biomedical [30,31], petrochemical [32,33], astronomy [34], and so on [35,36]. For determination of chicken meat spoilage, or specifically, total viable counts (TVC) in meats, both infrared (IR) and near infrared (NIR) spectroscopy have been investigated [13]. The principle for such detections was generally based on scrutinizing into chemical variations of meat components that were closely related with bacterial metabolism during storage. With the depletion of glucose and other simple carbohydrates by the growth of bacteria during storage, proteolysis in meat provides lots of free peptides and free amino acids as good source of energy to be utilized by the bacteria. Furthermore, a consortium of chemicals including volatile esters, alcohols, ketones and compounds containing sulfur is produced, and this complex mixture can contribute to the onset of off-flavours and finally putrid odors [37]. Spoilage of meat is also featured by gradual formation of slime due to synthesis of polysaccharides. The above-mentioned chemical changes can be captured and reflected in the infrared spectra and relevant changes in spectra can be utilized to be correlated with actual bacterial loads using chemometric methods. Ellis et al. [38] proved the efficiency of Fourier transform infrared (FT-IR) spectroscopy for detection of TVC using

* Corresponding author. Tel.: +353 1 7167342; fax: +353 1 7167493.
E-mail address: dawen.sun@ucd.ie (D.-W. Sun).
URLS: http://www.ucd.ie/refrig, http://www.ucd.ie/sun (D.-W. Sun).

0039-9140/$ - see front matter © 2012 Elsevier B.V. All rights reserved.
http://dx.doi.org/10.1016/j.talanta.2012.11.042

partial least square (PLS) regression and further investigation of several wavelengths selected by both genetic algorithms and genetic programming revealed that the change of free amino acids that can be picked up by FT-IR spectroscopy is closely related with spoilage of chicken meat. Lin et al. [37] studied the feasibility of visible and short-wavelength near-infrared (SW-NIR) diffuse reflectance spectroscopy. They found that principal component analysis (PCA) was able to sense slightly over one log cycle variation of total aerobic plate counts in chicken and the microbial loads can be well predicted using PLS regression with correlation coefficients and standard error of prediction of 0.91 and 0.48 log10 colony forming units per gram (log10 CFU per gram). Instead of using comminuted samples, Alexandrakis et al. [39] applied both FT-IR and NIR spectroscopy for measurement of TVC in intact chicken fillets. Their finding agreed well with the above two studies and combinative use of FT-IR and NIR spectroscopy further illustrated their competence.

Although vibrational spectroscopic methods have been used successfully in determining total viable counts (TVC) in meats as discussed above, they only detect small portions of the samples, so-called "point" detection, and such nature significantly limits their widespread applications. Most recently, an emerging method, hyperspectral imaging, was adopted by Grau et al. [40] to study the spoilage of chicken breast muscle in the wavelength bands between 400 and 1000 nm. By combining the strengths of computer vision [41–43] and spectroscopic technique, this emerging technique has the unique advantage that it can not only provide spectral information, but can also provide spatial information, and thus it is able to scan the whole surface of the product. However, despite the encouraging findings above, the precision for predicting TVC in chicken meat should be further improved. It was noticed that the above study [40] only used absorbance as spectral parameters, however, reflectance and Kubelka–Munk function/unit are also used in many applications as candidate spectral parameters [44–46]. In addition, to the best of the knowledge of the authors, no studies have been conducted to visualize the distribution of TVC on meats. Therefore, the objective of this study was to compare the three spectral parameters, i.e., reflectance (R), absorbance (A) and Kubelka–Munk (K–M) to improve the precision of calibration models for quantifying bacterial loads on chicken meat in the NIR wavelength range of 910–1700 nm other than in the shorter wavelength range. Meanwhile, the developed models were to be employed for visualization of TVC on chicken meat.

2. Materials and methods

2.1. Chicken samples and microbiological tests

'Chicken breast fillets packed in sealed plastic trays ($n=12$) were transferred to laboratory within 30 min upon purchase from a local supermarket. These packages were then stored in a refrigerator at 4 °C for use until the onset of obvious organoleptic spoilage, i.e., when the production of malodorous volatiles and visible slime were observed. Image acquisition and microbiological tests for these samples were carried out at storage days 0, 1, 2, 3, 4, 5, 6, 7, 7.5, 8, 8.5, and 9. On each day of experiment, fillets were removed from one package and cut aseptically into six to nine fractions each with a thickness of ~5 mm and weight of ~10 g. To avoid contamination during image acquisition, these prepared samples were transferred into individual sterile Petri dishes. After image acquisition, microbiological tests were implemented immediately to determine the total viable counts in each sample using standard spread plate technique. Each meat sample was put into ~90 ml buffered peptone water (BPW; CM0509, Oxoid, UK) after which the mixture was then homogenized to form the initial dilution. Series dilutions were also made by adding 1 ml of suspension into 9 ml BPW. Subsequently, 0.1 ml aliquots of appropriate dilution in duplicates were inoculated onto prepared plate count agar (CM0325, Oxoid, UK) and spread homogeneously on the agar surface. After setting, the plates were inverted and incubated at 35 °C for 48 h. All the colonies appearing on the plates were then counted, but only those whose colony count fell between 25 and 250 were considered reliable and used for calculation of final loads. As a result, totally 49 samples were obtained and the microbial loads were recorded in log10 CFU per gram.

2.2. Hyperspectral imaging systems

After taken out from the refrigerator, prepared samples were allowed to reach room temperature (21 ± 1 °C) for 10–15 min to avoid the effect from temperature. During image acquisition, a laboratory-based near-infrared (NIR) hyperspectral imaging system (910–1700 nm), as described in some other studies [47–49], was employed. Briefly, meat samples together with the Petri dishes were put onto the translation stage. The translation stage, which was driven by a stepper motor (GPL-DZTSA-1000-X, Zolix Instrument Co., China), moved at a speed of 44 mm s^{-1}. Sample images were taken when the light provided by two tungsten-halogen lamps (500 W, V-light, Lowel Light Inc., USA) were reflected from the meat surface, dispersed in a spectrograph (ImSpector N17E, Spectral Imaging Ltd., Oulu, Finland), projected to a CCD camera (Xeva 992, Xenics Infrared Solutions, Belgium) and then transformed into a digital signal by an image acquisition software (SpectralCube, Spectral Imaging Ltd., Finland) installed on a personal computer. For each sample, the image acquisition time was very short (approximately 3 s), therefore the heating effect of the light source on meat surface could be reasonably neglected. The spectral profiles of the resulting images, i.e., hypercubes, covered a spectral range of 910–1700 nm with ~3.34 nm interval. Due to different spatial scanning settings at different days of experiment, the spatial dimension of the images varied from 284 × 320 to 342 × 320 pixels, where 320 is the fixed width of the images with the other values indicating the number of lines scanned. However, the variations in image sizes or specifically the number of lines scanned should not influence the subsequent data processing since a larger spatial dimension simply meant more background information was included and in the subsequent data processing, only image of the meat portions were manipulated for model calibration.

2.3. Image processing and extraction of spectra

Raw hyperspectral images (I) in radiance acquired by the pushbroom near-infrared hyperspectral imaging system were calibrated into reflectance images (R) with the aid of two additional hyperspectral images I_w and I_d for a standard white tile (~100% reflectance) and dark current (~ 0% reflectance), respectively. The formula applied was as follows:

$$R = \frac{I - I_d}{I_w - I_d} \quad (1)$$

For each of the obtained R images, a binary image called mask was created by thresholding a gray image that was produced by subtracting a high reflectance image at band 15 using a low reflectance image at band 150. During masking, a global threshold value of 0.22 was employed. The mask was applied to the calibrated reflectance image to suppress the background to zero. The spectral profiles of the pixels in the retained meat portions of the image were transformed into absorbance (A) and K–M units using the following equations:

$$A = -\log_{10} R \quad (2)$$

$$K - M = \frac{(1-R)^2}{2R} \quad (3)$$

The average of the spectra in the masked region (i.e., meat portion) of each image was extracted as a representative spectrum for the meat sample. Accordingly, three spectral calibration sets with different units, i.e., *R*, *A* and K–M, were obtained and used, together with the measured bacterial loads to establish partial least squares regression models, which were then denoted as R-PLSR, A-PLSR and KM-PLSR models, respectively.

2.4. Establishment and evaluation of PLS models

Linear PLSR models were constructed to correlate the spectra and the microbial counts of samples. The spectra utilized here included two categories, i.e., full-wavelength spectra and simplified spectra where limited number of wavelengths was selected by stepwise regression. Therefore, two categories of calibration models were built. Moreover, these models were further validated using leave-one-out full cross-validation. To assess the performance of developed models, several parameters, including correlation coefficients (R) and root mean squared errors (RMSEs) were calculated for calibration and cross-validation, respectively [50]. Sample outliers were detected in light of Student's *t*-test, where samples with $t > 2$ were excluded from the calibration set [51], though some studies also used 2.5 as a thresholding *t* value [52]. In addition, the root mean squared errors for calibration (RMSEC) and cross-validation (RMSECV) were calculated and, in particular, RMSECV was employed to divide standard deviation (SD) of measured bacterial counts in the calibration set, resulting in a parameter named ratio of performance to deviation (RPD) [53]. An RPD value lower than 1.5 would indicate that the model established is not acceptable; if it lies between 2 and 2.5, a feasible model for rough assessment purpose is believed to have been produced; and a model is considered as good or excellent when its RPD value is smaller (but larger than 2.5) or larger than 3, respectively [14,39]. Besides, RMSECV was also used in determining the optimal number of latent variables (i.e., the rank), where the one corresponding to the lowest RMSECV was allocated.

2.5. Visualization maps

When the best PLSR models (both full-wavelength or simplified models) based on different spectral signatures were finally confirmed, they were applied for predicting bacterial loads in each pixel of the sample images. Specific procedures for such predictions have been explained in detail elsewhere [49]. The resulting two-dimensional images with predicted bacterial loads comprising the meat portions were shown in color, where the total viable counts linearly corresponded to the color scale. In this way, by checking the color variation in the developed map, one can easily access the predicted distribution of bacterial loads in the meat.

3. Results and discussion

3.1. Microbiological tests

A good variation within microbial loads was gained in this study. Total bacterial counts of chicken varied from 3.15 to 8.03 log10 CFU per gram, which was comparable to what had been reported in previous studies [37,38]. The great variations within TVC loads could be attributed to the long-time storage of samples, which were preserved until onset of sensible spoilage.

3.2. Spectra

Near infrared spectroscopy is a technology based on absorption of light by molecules, therefore, to have a better expression of the absorbance bands, the absorbance spectra are shown in Fig. 1. As can be seen, there are two strong absorption bands (downward peaks) centered at 971 and 1197 nm, which can be ascribed to the presence of water and fatty acids or fat, respectively [54–56]. Also noticed were nearly flat but well-separated curves over the wavelength range between 1415 and 1635 nm. Within this range, there was pronounced absorption of water due to intensive O–H first stretching overtone at around 1450 nm [26]. Moreover, water was believed to dominate in this wavelength range, thus the presence of some other chemicals, e.g., protein, which should result in peaks between 1510 and 1550 nm due to the first N–H stretching overtone [57,58], was not clearly reflected in the spectra.

3.3. PLSR models based on full wavelengths

Three types of PLSR calibration models were established based on reflectance, absorbance and K–M spectral profiles in the full wavelength range. These models were denoted as RF-PLSR, AF-PLSR and KMF-PLSR models, respectively. The performance of the best models of each type is shown in Table 1. It was demonstrated that the best AF-PLSR model had better performance than those of the other two types, with the highest correlation coefficients of 0.97 and 0.93 as well as the lowest RMSEs of 0.37 and 0.57 log10 CFU per gram for calibration and cross validation, respectively. Besides, the RPD value for the AF-PLSR model was also the largest among the three though the corresponding rank (7) was slightly higher than the other two. The KMF-PLSR model was the second best and this model was featured by a simple structure as indicated by the lowest number

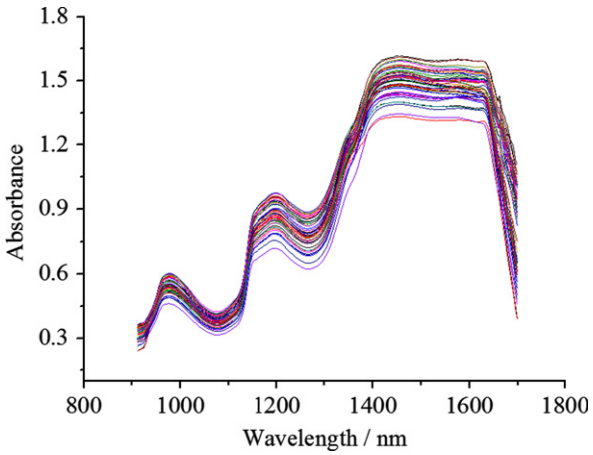

Fig. 1. Absorbance spectra of the chicken breast fillet samples.

Table 1
Performance of optimal full-wavelength PLSR models based on different spectral parameters.

Spectral parameters	Calibration		Cross validation		Rank	RPD
	R_c	RMSEC (log10 CFU per gram)	R_{cv}	RMSECV (log10 CFU per gram)		
R	0.92	0.55	0.88	0.71	6	2.05
A	0.97	0.37	0.93	0.57	7	2.60
K–M	0.96	0.38	0.92	0.59	5	2.55

(5) of latent variables employed. The correlation coefficients and RMSEs were all very close to those for the AF-PLSR model with only a slight difference in corresponding statistics. Comparatively, the RF-PLSR model had the poorest performance where much higher RMSEs were found. Nevertheless, the optimum RF-PLSR model was still qualified for possible prediction, i.e., rough screening, because the RPD value from RF-PLSR model was higher than 2 [25]. Moreover, more appreciated RPD values which were both higher than 2.5 for AF-PLSR and KMF-PLSR models indicated that these two models were applicable for future prediction with good precision [25,59].

3.4. PLSR models based on selected wavelengths

The established PLSR models based on full wavelengths had illustrated the suitability of the NIR hyperspectral imaging system for either coarse or accurate prediction of bacterial loads on chicken in future applications. However, it could be very difficult or not realistic for such applications to be developed into online routines due to huge data (image) size and hardware restrictions [60]. To meet the need for online sensing, one feasible solution would be to develop multispectral imaging systems where a great number of wavelengths (>200) in hyperspectral imaging systems can be reduced to less than 10, thus resulting in substantially reduced image sizes that help alleviate hardware requirements and computing loads. In this study, stepwise regression was employed to allocate important wavelengths aiming to establish simplified PLSR models based on the three spectral attributes. The significance level for the selection of important wavelengths was 5%.

Five wavelengths selected for the simplified PLSR model based on reflectance spectra (RS-PLSR) included 954, 957, 1138, 1148 and 1328 nm. Among the five wavelengths, 954 and 957 nm are mainly associated with the second overtone of the stretching OH bond, which can be attributed to the presence of water [61–63], the dominant component in raw meat. However, amines due to the C–N second overtone may also have contributed to the spectral absorbance in these two bands [57]. Moreover, the remaining three wavelengths selected for RS-PLSR model can be assigned to second overtone symmetrical stretching of C–H, which are closely related with amino acids [64]. These selected wavelengths provided further confirmation for previous studies which concluded that, during chicken storage and spoilage, the most important chemical change picked up by near-infrared spectroscopic analysis was the variation of amides and amines [37–39,65]. With the selected wavelengths, the RS-PLSR model gave better performance than when full wavelengths were utilized although the modeling errors for calibration were slightly increased (refer to Table 2). The RPD value was also enhanced to 2.11 from 2.05.

More spectral bands were selected for the establishment of simplified calibration models based on absorbance data (AS-PLSR) and the ten wavelengths (961, 1054, 1081, 1084, 1191, 1198, 1201, 1208, 1218 and 1328 nm) also provided potential indication of changes in chemicals, namely, water, amides and amino acids [57], which can account for spoilage of raw chicken fillets. Similar to the case of reflectance models, the correlation coefficients for calibration in the AS-PLSR model dropped to 0.96, meanwhile, an increase in RPD from 2.60 for the AF-PLSR model to 2.75 for the AS-PLSR model was also found. When it comes to simplified models based on K–M parameters (KMS-PLSR models), a total of seven wavelengths (1145, 1458, 1522, 1659, 1666, 1669 and 1672 nm) were allocated. Using these wavelengths, an excellent model was achieved with a RPD value of 3.02 (higher than the threshold of 3 for excellence). The great enhancement of the model was also reflected in the coefficients for cross validation, which was augmented from 0.92 for the KMF-PLSR model to 0.94 for the KMS-PLSR model.

Compared to the full wavelength models, the simplified models turned out to be more robust, which was indicated by smaller difference in both correlation coefficients and root mean squared errors for both calibration and cross validation. The improvement in model capability can probably be attributed to the elimination of the uninformative or even misleading wavelengths for explaining the spoilage process of raw chicken. In addition, the reduction of spectral multicollinearity could also be part of the reasons for model enhancement.

3.5. Visualization of total viable counts

Visualization allows for a novel way for intuitive perception of the distribution of targets under study. In this study, all the PLSR models (including both optimal full wavelength models and simplified models based on reflectance, absorbance and K–M spectral profiles) were applied to the images in the sample set. However, only one image, as an example, is visualized in Fig. 2 for illustration purpose. In Fig. 2, the first row was the visualization result after applying optimal full wavelength models (i.e., RF-PLSR, AF-PLSR and KMF-PLSR models, respectively), while the second row gives the predicted distribution by simplified models (i.e., RS-PLSR, AS-PLSR and KMS-PLSR models, respectively). There are also two identical color scales besides the visualization map to explain the meaning of different colors in the maps of each row. Specifically, the blue end of a color bar indicates very low bacterial load, 0 log10 CFU per gram in this case, while the red end designates a very high level of total viable count, 10 log10 CFU per gram. Thus, by looking into the color of each pixel in the meat portion of the map, one can immediately tell the bacterial count at that specific location by referring back to the color scale.

Generally, the distribution maps produced a unanimous trend for bacterial distribution on the same meat surface except the one produced by the AS-PLSR model. There were low bacterial loads in the centre of the meat but high loads of sporadic portions in other parts. The consistency was believed to have been ascertained by the goodness or excellence of established calibration models which accounted for the major linear relationship between the variations of microbial loads in meat during storage and the corresponding changes in spectral profiles. Another interesting phenomenon was that the full wavelength models tended to produce much smoother maps than the simplified models did. Since the prediction was achieved by inner product of spectra and fixed regression coefficients, the use of all the wavelengths would minimize the effect from random noise, which can be called a

Table 2
Performance of simplified PLSR models based on different spectral parameters.

Spectral profiles	Wavelengths selected (nm)	Calibration		Cross validation		RPD
		R_c	RMSEC (log10 CFU per gram)	R_{cv}	RMSECV (log10 CFU per gram)	
R	954, 957, 1138, 1148, 1328	0.91	0.59	0.88	0.69	2.11
A	961, 1054, 1081, 1084, 1191, 1198, 1201, 1208, 1218, 1328	0.96	0.42	0.93	0.54	2.75
K–M	1145, 1458, 1522, 1659, 1666, 1669,1672	0.96	0.40	0.94	0.50	3.02

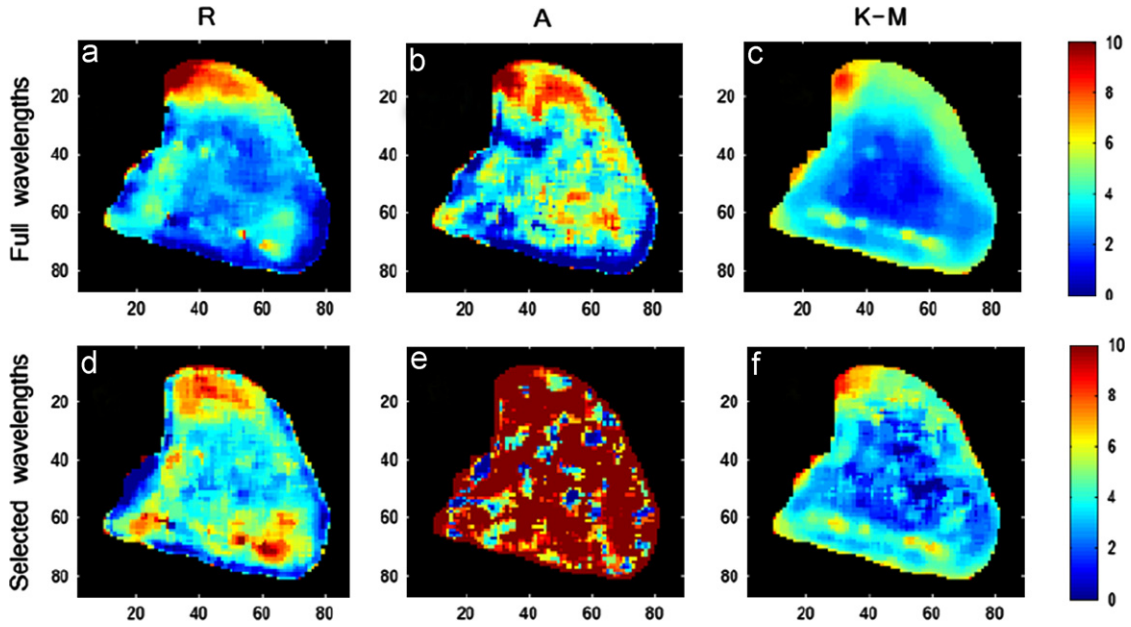

Fig. 2. Distribution maps of TVC in a representative meat sample after applying different PLSR models (a: RF-PLSR model; b: AF-PLSR model; c: KMF-PLSR model; d: RS-PLSR model; e: AS-PLSR model; and f: KMS-PLSR model). Colors in the two identical scales on the right of each row of maps are shown to indicate bacterial loads (in log10 CFU per gram). The black color in each map, but not shown in the scales, is used specically for indication of background. The numbers along each map give the spatial dimensions (number of pixels) of the sample. The sample was from Day 0 and the corresponding bacterial count was 3.27 log10 CFU per gram. (For interpretation of the references to color in this figure legend, the reader is referred to the web version of this article.)

smoothing effect, but this was very limited for models based on selected wavelengths, which were more vulnerable to random noise and abnormalities. However, confusing information was also noticed. For example, the edges of maps for RF-PLSR, RS-PLSR and AF-PLSR models tended to be of low-level bacterial counts while the margin of maps for PLSR models based on K–M spectra showed higher loads. This confliction was hard to explain since the real distribution of bacteria on the meat edges was not available, but the imperfection of images due to edge effect could be one of the reasons. Besides, the discrepancy in displaying bacterial counts in similar regions of the meat sample probably could be ascribed to the variation of model performance. In other words, such difference depended mainly on how close these models can make a prediction to the true value.

In terms of the prediction map which was developed by applying AS-PLSR models and was alien to the other five maps, the bacterial loads at the overwhelming majority of the sample surface were substantially overestimated as indicated by the large area with dark red color. Such a distribution map was unreliable since for meat with a total viable count of 3.27 log10 CFU per gram should not have a large area of surface that has bacterial loads close to 10 log10 CFU per gram (very small fractions of such area may exist due to unexpected contamination), because meat with such a large area of high TVC values could have been concluded as spoiled. Further evidence for the deficiency of this model was that the bacterial load of this sample was predicted as 10.58 log10 CFU per gram, which was far more than the reference value. The reason why a good AS-PLSR model could not produce a good visualization map could be the poor adaptability of the model itself. By investigating the output of the AS-PLSR model, very large regression coefficients, ranging from −1001.78 to 1404.52 (figure not shown), were found. Based on the huge fluctuation of regression coefficients, which can be considered as weights for spectral profiles at specific wavelengths when calculating the prediction, a trivial change in the spectral parameter can result in dramatic difference in the final prediction, so-called the butterfly effect [66]. Though using different bands may modify this exaggeration, the extent, i.e., whether in a positive way or in a negative aspect, is not controllable since the shift of spectral response due to random noise is hard to predict. Briefly, the AS-PLSR model, though good, requires too rigid accuracy on spectra and its successful applications relies heavily on the hardware producing fine spectra. The high-quality spectra for building the AS-PLSR model was achieved by computing the average spectra of the meat samples, where most of random noise was believed to have been removed. Other models did not produce regression coefficients of large values and, therefore, they were more robust to noise and had better adaptability. Accordingly, in some sense, the production of visualization maps can be considered as an effective way for model validation. In addition, some abnormalities in the raw image, i.e., dead pixels, spectral spikes as well as specular reflectance, etc., could also have influenced the model performance. However, they are normally separate individuals in minority and can be removed by median filtering (except specular reflectance which usually takes up more pixels). Specular reflectance in images should be taken special care of during image processing in order to establish a better model and to further reveal the distribution of targets under investigation.

4. Conclusions

Near-infrared hyperspectral imaging (910–1700 nm) was demonstrated to be potential for quantifying total viable counts in chicken fillet samples in a non-destructive and rapid way. Optimal full-wavelength calibration models based on each of the spectral attributes, i.e., reflectance, absorbance and K–M, produced reasonable performance. In particular, models based on absorbance and K–M spectra were good with RPD values higher than 2.5. The best full wavelengths model turned out to be the PLS regression model based on absorbance spectra. Furthermore, simplified models were also established after selecting some wavelengths by stepwise regression. All the simplified models had higher RPD values than the respective full-wavelength models, and the best model was obatined for the prediction based on K–M spectra. The optimal model (KMS-PLSR)

resulted in high correlation coefficients of 0.96 and 0.94 as well as low root mean squared errors of 0.40 and 0.50 log10 CFU per gram for calibration and cross validation, respectively. Moreover, large RPD (3.02) suggested the excellence of the KMS-PLSR model. The production of prediction maps could be used to visualize the distribution of microbial loads on the meat surface and it was pointed out that the quality of distribution map relies on the quality of the image and the robustness and adapability of established models. Specifically, a model with good statistics would sometimes give misleading or obviously untrustable distribution of the targets, while application of a moderate model may, on the contrary, be able to produce acceptable mapping. Visualization maps can provide efficient alternatives for model evaluation. Future work should be carried out to reduce image noise and to eliminate image flaws (i.e., dead pixels, spectral spikes, specular reflectance, etc.) so that the image quality and probably the model accuracy could be enhanced. In addition, multispectral imaging systems are also suggested to be developed and applied for online detection.

Acknowledgments

China Scholarship Council and University College Dublin are acknowledged for supporting this study via CSC-UCD Scholarship Scheme. Dr. Amalia Scannell, Dr. Noha Morcy, Dr. Des Walsh and Dr. Gamal ElMasry are gratefully thanked for kind assistance and suggestions.

References

[1] L.R. Ferguson, Meat Sci. 84 (2010) 308–313.
[2] K Mc Donald, D-W Sun, Effect of evacuation rate on the vacuum cooling process of a cooked beef product, J. Food Eng 48 (3) (2001) 195–202, http://dx.doi.org/10.1016/S0260-8774(00)00158-8.
[3] LJ Wang, D-W Sun, Modelling vacuum cooling process of cooked meat - part 1: analysis of vacuum cooling system, Int. J. Refrigeration-Revue Internationale du Froid 25 (7) (2002) 854–861, http://dx.doi.org/10.1016/S0140-7007(01)00094-9, Article Number: PII S0140-7007(01)00094-9.
[4] B Li, D-W Sun, Effect of power ultrasound on freezing rate during immersion freezing of potatoes, J. Food Eng. 55 (3) (2002) 277–282, http://dx.doi.org/10.1016/S0260-8774(02)00102-4, Article Number: PII S0260-8774(02)00102-4.
[5] D-W Sun, ZH Hu, CFD simulation of coupled heat and mass transfer through porous foods during vacuum cooling process, Int. J. Refrigeration-Revue Internationale du Froid 26 (1) (2003) 19–27, http://dx.doi.org/10.1016/S0140-7007(02)00038-5, Article Number: PII S0140-7007(02)00038-5.
[6] D-W Sun, B Li, Microstructural change of potato tissues frozen by ultrasound-assisted immersion freezing, J. Food Eng. 57 (4) (2003) 337–345, http://dx.doi.org/10.1016/S0260-8774(02)00354-0, Article Number: PII S0260-8774(02)00354-0.
[7] D-W Sun, LY Zheng, Vacuum cooling technology for the agri-food industry: Past, present and future, J. Food Eng. 77 (2) (2006) 203–214, http://dx.doi.org/10.1016/j.jfoodeng.2005.06.023.
[8] D-W Sun, IW Eames, Performance characteristics of HCFC-123 ejector refrigeration cycles, Int. J. Energ. Res. 20 (10) (1996) 871–885, http://dx.doi.org/10.1002/(SICI)1099-114X(199610)20:10〈871::AID-ER201〉3.3.CO;2-W.
[9] D-W Sun, IW Eames, S Aphornratana, Evaluation of a novel combined ejector-absorption refrigeration cycle .1. Computer simulation, Int. J. Refrig.-Revue Internationale du Froid 19 (3) (1996) 172–180, http://dx.doi.org/10.1016/0140-7007(96)00010-2.
[10] D-W Sun, Solar powered combined ejector vapour compression cycle for air conditioning and refrigeration, Energ. Conversi. Manageme 38 (5) (1997) 479–491, http://dx.doi.org/10.1016/S0196-8904(96)00063-5.
[11] D-W Sun, Comparison of the performances of NH3-H2O, NH3-LiNO3 and NH3-NaSCN absorption refrigeration systems, Energ. Convers. Manage 39 (5–6) (1998) 357–368, http://dx.doi.org/10.1016/S0196-8904(97)00027-7.
[12] D-W. Sun, Comparative study of the performance of an ejector refrigeration cycle operating with various refrigerants, Energ. Conversi. Manageme. 40.
[13] D.I. Ellis, R. Goodacre, Trends Food Sci. Technol. 12 (2001) 414–424.
[14] C. Thomas, T. McMeekin, Appl. Environ. Microb. 41 (1981) 492–503.
[15] C.D. Zook, F.F. Busta, in: K.R. Richard (Ed.), Encyclopedia of Food Microbiology, Elsevier, Oxford, UK, 1999, pp. 2176–2180.
[16] D.A. Bautista, in: K.R. Richard (Ed.), Encyclopedia of Food Microbiology, Elsevier, Oxford, UK, 1999, pp. 80–88.
[17] T. Sakakibara, S. Murakami, K. Imai, Anal. Biochem. 312 (2003) 48–56.
[18] L. Ramsahoi, A. Gao, M. Fabri, J.A. Odumeru, J. Dairy Sci. 94 (2011) 3279–3287.
[19] A. Dolan, C.M. Burgess, T.B. Barry, S. Fanning, G. Duffy, J. Microbiol. Methods 77 (2009) 1–7.
[20] N. Garrec, F. Dilasser, A.M. Pourcher, S. Perelle, P. Fach, J. Microbiol. Methods 55 (2003) 763–773.
[21] N. Krämer, C. Löfström, H. Vigre, J. Hoorfar, C. Bunge, B. Malorny, Int. J. Food Microbiol. 145 (Suppl. 1) (2011) S86–S95.
[22] I. Wesley, W. Muraoka, Food Bioprocess. Technol. 4 (2011) 616–623.
[23] S. García, N. Heredia, Food Bioprocess. Technol. 4 (2011) 624–630.
[24] V. Bellon-Maurel, A. McBratney, Soil Biol. Biochem. 43 (2011) 1398–1410.
[25] B.M. Nicolaï, K. Beullens, E. Bobelyn, A. Peirs, W. Saeys, K.I. Theron, J. Lammertyn, Postharvest Biol. Technol. 46 (2007) 99–118.
[26] N. Prieto, R. Roehe, P. Lavín, G. Batten, S. Andrés, Meat Sci. 83 (2009) 175–186.
[27] L. Magwaza, U. Opara, H. Nieuwoudt, P. Cronje, W. Saeys, B. Nicolaï, Food Bioprocess. Technol. 5 (2012) 425–444.
[28] A. Chudnovsky, E. Ben-Dor, Sci. Total Environ. 393 (2008) 198–213.
[29] A. Vergnoux, M. Guiliano, Y. Le Dréau, J. Kister, N. Dupuy, P. Doumenq, Sci. Total Environ. 407 (2009) 2390–2403.
[30] H.H. Mantsch, L.-P. Choo-Smith, R.A. Shaw, Vib. Spectrosc. 30 (2002) 31–41.
[31] A. Kudelski, Talanta 76 (2008) 1–8.
[32] S. Macho, M.S. Larrechi, Trends Anal. Chem. 21 (2002) 799–806.
[33] M.V. Reboucas, J.B.d. Santos, D. Domingos, A.R.C.G. Massa, Vib. Spectrosc. 52 (2010) 97–102.
[34] K. Kawaguchi, Handbook of Vibrational Spectroscopy, John Wiley & Sons, Ltd., 2006.
[35] R. Vogel, F. Siebert, Curr. Opin. Chem. Biol. 4 (2000) 518–523.
[36] R. Schweitzer-Stenner, Vib. Spectrosc. 42 (2006) 98–117.
[37] M. Lin, M. Al-Holy, M. Mousavi-Hesary, H. Al-Qadiri, A.G. Cavinato, B.A. Rasco, Lett. Appl. Microbiol. 39 (2004) 148–155.
[38] D.I. Ellis, D. Broadhurst, D.B. Kell, J.J. Rowland, R. Goodacre, Appl. Environ. Microb. 68 (2002) 2822–2828.
[39] D. Alexandrakis, G. Downey, A. Scannell, Food Bioprocess. Technol. 5 (2012) 338–347.
[40] R. Grau, A.J. Sánchez, J. Girón, E. Iborra, A. Fuentes, J.M. Barat, Food Res. Int. 44 (2011) 331–337.
[41] D-W Sun, T Brosnan, Pizza quality evaluation using computer vision – part 1 - Pizza base and sauce spread, J. Food Eng. 57 (1) (2003) 81–89, http://dx.doi.org/10.1016/S0260-8774(02)00275-3, Article Number: PII S0260-8774(02)00275-3.
[42] CX Zheng, D-W Sun, LY Zheng, Recent applications of image texture for evaluation of food qualities - a review, Trends Food Scie Technol 17 (3) (2006) 113–128, http://dx.doi.org/10.1016/j.tifs.2005.11.006.
[43] CX Zheng, D-W Sun, LY Zheng, Recent developments and applications of image features for food quality evaluation and inspection - a review, Trends Food Scie Technol 17 (12) (2006) 642–655, http://dx.doi.org/10.1016/j.tifs.2006.06.005.
[44] B.M. Nicolaï, K.I. Theron, J. Lammertyn, Chemometr. Intell. Lab. Syst. 85 (2007) 243–252.
[45] M. Otsuka, Powder Technol. 141 (2004) 244–250.
[46] J. Moros, M.J. Martínez-Sánchez, C. Pérez-Sirvent, S. Garrigues, M. de la Guardia, Talanta 78 (2009) 388–398.
[47] D. Barbin, G. Elmasry, D.-W. Sun, P. Allen, Meat Sci. 90 (2012) 259–268.
[48] G. ElMasry, D.-W. Sun, P. Allen, J. Food Eng. 110 (2012) 127–140.
[49] M. Kamruzzaman, G. ElMasry, D.-W. Sun, P. Allen, Anal. Chim. Acta 714 (2012) 57–67.
[50] V. Sinija, H. Mishra, Food Bioprocess. Technol. 4 (2011) 136–141.
[51] M. Bonierbale, W. Grüneberg, W. Amoros, G. Burgos, E. Salas, E. Porras, T.z. Felde, J. Food Compos. Anal. 22 (2009) 509–516.
[52] F. Guy, S. Prache, A. Thomas, D. Bauchart, D. Andueza, Food Chem. 127 (2011) 1280–1286.
[53] B. Kemps, L. Leon, S. Best, J. De Baerdemaeker, B. De Ketelaere, Biosyst. Eng. 105 (2010) 507–513.
[54] I. González-Martı´n, C. González-Pérez, N. Alvarez-Garcı´a, J.M. González-Cabrera, Meat Sci. 69 (2005) 243–248.
[55] V.M. Fernández-Cabanás, O. Polvillo, R.R. Rodríguez-Acuña, B. Botella, A. Horcada, Food Chem. 124 (2011) 373–378.
[56] P. Williams, in: P. Williams, K. Norris (Eds.), Near Infrared Technology in the Agriculture and Food Industries, American Association of Cereal Chemists, Minnesota, USA, 2001.
[57] C.E. Miller, in: P. Williams, K. Norris (Eds.), Near Infrared Technology in the Agricultural and Food Industries, American Association of Cereal Chemists, Minnesota, USA, 2001, pp. 19–37.
[58] D. Alomar, C. Gallo, M. Castañeda, R. Fuchslocher, Meat Sci. 63 (2003) 441–450.
[59] I. González-Martín, J. Hernández-Hierro, M. Bustamante-Rangel, N. Barros-Ferreiro, Anal. Bioanal. Chem. 386 (2006) 1553–1558.
[60] Y.-Z. Feng, D.-W. Sun, Crit. Rev. Food Sci. Nutr. 52 (2012) 1039–1058.
[61] H. Büning-Pfaue, Food Chem. 82 (2003) 107–115.
[62] X.-L. Li, Y. He, Food Bioprocess. Technol. 3 (2010) 651–661.
[63] F. Zhu, S. Cheng, D. Wu, Y. He, Food Bioprocess. Technol. 4 (2011) 597–602.
[64] J. Workman, L. Weyer, Practical Guide to Interpretive Near-Infrared Spectroscopy, CRC, Boca Raton, 2008.
[65] D. Alexandrakis, N. Brunton, G. Downey, A. Scannell, Food Bioprocess. Technol. 5 (2012) 1917–1923.
[66] S. Wolfram, in: S. Wolfram (Ed.), A New Kind of Science, Wolfram Media Inc., 2002, pp. 304–314.